separations

Article

Fabrication and Characterization of Sulfonated Carbon Materials and Chitosan-Derived Functioned Carbon via Schiff's Base Process for Separation Purposes

Ali S. Alghamdi [1,2], Kareem Yusuf [1,2], Mohamed A. Habila [1,2,*] and Zeid A. ALOthman [1]

[1] Advanced Materials Research Chair (AMRC), Department of Chemistry, College of Science, King Saud University, P.O. Box 2455, Riyadh 11451, Saudi Arabia; kmahmoud@ksu.edu.sa (K.Y.); zaothman@ksu.edu.sa (Z.A.A.)
[2] Department of Chemistry, College of Science, King Saud University, P.O. Box 2455, Riyadh 11451, Saudi Arabia
* Correspondence: mhabila@ksu.edu.sa; Tel.: +966-1-4674-198; Fax: +966-1-4675-992

Abstract: The Schiff bases reaction is applied to form various functioned carbon structures using renewable carbon from waste sources, Chitosan, 4-Amino-3-hydroxy-napthalene-1-sulphnic acid, and dimethyl amino benzaldehyde as starting materials. The formed functioned carbons were characterized by TEM, FTIR, XRD, and surface area analysis to assess their morphology, structure, porosity, and surface functional groups. In addition, the chromatographic-based thermodynamic analysis is applied to evaluate the surface energy and thermodynamic parameters during the separation of hydrocarbon species. Results indicated the formation of various carbon structures in convex-like shapes with diameters between 600 nm and 1500 nm, including side-building edges of diameter between 100 nm and 316 nm. The formed functioned carbon surfaces are rich with O-H, N=C, C=C, C=O, and C=S groups, as indicated by the FTIR. The function carbons are named carbon coated with Chitosan-derived covalent organic layer (C@Chitosan-COL) as well as Schiff's base-derived sulfonated carbon (Schiff's-C-S) in relation to the applied starting materials. The chromatographic-based thermodynamic analysis showed that the entropy changes of adsorption (ΔS_A) increased with increasing chain length demonstrating less random movement and higher adsorption in both materials. The fabricated C@Chitosan-COL and Schiff's-C-S showed an efficient separation of hydrocarbon mixture including n-Nonane, n-Decane, n-Undecane, and n-Dodecane.

Keywords: schiff's base; carbon materials; hydrocarbon separation; gas chromatography; adsorption; thermodynamic parameters

check for updates

Citation: Alghamdi, A.S.; Yusuf, K.; Habila, M.A.; ALOthman, Z.A. Fabrication and Characterization of Sulfonated Carbon Materials and Chitosan-Derived Functioned Carbon via Schiff's Base Process for Separation Purposes. *Separations* **2023**, *10*, 475. https://doi.org/10.3390/separations10090475

Academic Editor: Xin Zhang

Received: 12 July 2023
Revised: 19 August 2023
Accepted: 21 August 2023
Published: 30 August 2023

Copyright: © 2023 by the authors. Licensee MDPI, Basel, Switzerland. This article is an open access article distributed under the terms and conditions of the Creative Commons Attribution (CC BY) license (https://creativecommons.org/licenses/by/4.0/).

1. Introduction

Developments of materials with various structures and composites have become a vital trend to enhance the separation processes [1–3]. The separation technique is widely applied for industrial and environmental purposes. The separation processes of the analytes are the most crucial step in the analytical methods. The suitable separation process enables accurate detection and professional quantitative analysis [4,5]. However, the traditional techniques for separation, such as physical distillation, recrystallization, and preconcentration, consume high quantities of solvents and are classified as energy-demanding techniques. Recent research is focused on developing low-cost separation processes as alternatives to reduce energy consumption in real-field applications [6–9]. The adsorption process is classified as an effective and promised separation technique due to low operating costs as well as cheap starting materials [10,11].

The Schiff's bases derived materials are generally prepared from a condensation reaction between primary amines and carbonyl compounds (aldehydes or ketones). They were discovered for the first time in 1864 by Hugo Joseph. The constituent group (imine C=N)

has distinctive physical and chemical properties and wide applications in biochemistry, adsorption, pharmacology, catalysts, and separation chemistry as well [12]. Schiff's base modification has been widely applied for developing adsorbents for environmental and separation purposes [13–15]. In addition, Schiff's base is used to fabricate the covalent organic frameworks (COFs), producing a highly functioned material for separating organic compounds, which is exciting in industrial and environmental chemistry [16–18]. Schiff's base root for obtaining a covalent organic framework enables structure and surfaces functional group variation via selecting suitable starting materials [19,20]. For example, Li et al. have fabricated a covalent organic framework with sulfonic acid functional groups (TpPa–SO_3H using the solvothermal method, reporting highly active surface with functional groups including C–N, O=S=O, C=C, and C=O [21]. Peng et al. reported a method for introducing sulfonic acid for building modularly crystalline porous frameworks by mechanoassisted synthesis process of two sulfonated COFs yielding one-dimensional nanoporous channels decorated with pendant sulfonic acid groups [22]. In addition, it is involved in the fabrication of Pd loaded by Li et al. [23].

The presence of Chitosan in the entire structure of the materials orients functionality for more stable organic species due to amino and hydroxyl groups acting as H-bond donors/acceptors, enhancing the 3D network. Chitosan-based materials possess many advantages, such as hydrophilic character, high chemical reactivity, and efficient adsorption capacity [24,25]. However, the direct application of Chitosan is limited due to swelling and its tendency to dissolve in an acidic medium. Cross-linking-based derivatization or combination with other adsorbent materials improves the stability of Chitosan in the acidic medium as well as enhances their application as adsorbents [14,26,27]. Furthermore, the chitosan functional groups, such as amine and hydroxyl, enable easy modification and combination with other adsorbent textures [13,28,29]. The COFs-derived materials showed high hydrothermal stability because of the involvement of stable covalent bonds leading to better processability and applicability for various applications, including catalysis, water treatment, and separation [30–32]. The COFs-derived materials have been reported as preferred materials for stationary phases due to their stability as well as the high hydrophobic interaction based on the electron donor/acceptor between COFs surfaces and analytes mixtures [33–35]. However, the direct application as packing materials is limited because of the small crystal size and non-spherical shape. Therefore, the research strategies focus on incorporating the COFs with suitable support materials.

Recently, several functionalizations have been successfully developed via a modification to further improve the potential performances of MOFs and/or COFs to extend their applicability [36–43]. In addition, the silica is applied as fillers to facilitate column-packings with COFs. Furthermore, COFs are reported for combination with silica by crushing in methanol and mixing with silica to enable their performance as a stationary phase for liquid chromatographic separation, with high efficiency for separating xylene isomers and ethylbenzene. Liang et al. have fabricated graphene oxide/COFs by Schiff base coupling reaction between 1,3,5-tri(4-aminophenyl) benzene and 2,5-divinylterephthalaldehyde on the surface and between layers of GO, reporting effective performance for separation of naphthalene, 1-naphthylamine, and 1-naphthol from aqueous solution [44] Yola and Atar have developed titanium-based metal–organic framework (Ti-MOF, NH_2-MIL-125)@covalent organic frameworks (COFs) composite for the signal amplification which serves to the sense of antigen GL-3 using gold nanoparticle-functionalized graphitic carbon nitride nanosheets [45].

Chromatographic separation could be applied to evaluate the materials' surface behavior and investigate the thermodynamic properties. Chromatographic separation is the commonly used technique for the most precise analysis and separation of organic components in diverse research fields, including environmental engineering and industrial and pharmaceutical applications. The fundamental principle of the chromatographic system depends on the nature of the stationary phase, which could facilitate or retard the efficiency of mixtures separations. The surface functional groups and porosity, as well as

the nature of the entire skeleton of stationary phase materials, are the influencing factors that determine the chromatographic mechanism, which may involve various interactions, such as Vander Waals, dipole–dipole, hydrophilic or hydrophobic properties between the stationary phase and analytes mixtures. The reverse gas chromatography technique is widely used to study the physical and chemical properties and surface energy of individual substances and mixtures by analysis of quantities characterizing the chromatographic retention behavior of known volatile liquids and gases [46]. Various organic mixtures can be investigated to assess the thermodynamic properties of stationary phase materials. The thermodynamics enable accurate prediction of the developed adsorbent's performance and assess the mechanism of chromatographic separation. The process is operated by packing the developed material in a suitable column as stationary phases with various surface functional groups and evaluating them for different mixtures separation. Hydrocarbons are mainly composed of two elements, carbon and hydrogen. Light hydrocarbons are primary energy sources and raw materials for the production of some industrially essential chemicals, which mainly originate from the processing of petrochemicals or natural gas [47]. Separating the components of different hydrocarbons to meet various industrial needs is a crucial issue in chemical production [48,49].

The fractionation technique is commonly used to separate hydrocarbons based on their differences in boiling point. However, adsorption separation technology is also used as it has many advantages, such as energy saving and high efficiency, which has attracted wide attention in the research field [50–54]. Ban S et al. used different zeolites, mordenite, Y, β, and silicalite, to absorb and separate benzene in a benzene/propylene mixture. The research results showed high selectivity and high stability adsorption performance [55]. Asghar et al. performed a comparative study of the separation results of a mixture of alkane was carried out silica gel and new MWCNT–Silica gel nanocomposite, and the results showed better separation estimates and high sensitivity new MWCNT–Silica gel nanocomposite [56]. Andrea Speltini et al. prepared a novel application of pristine and functionalized Multi-Walled Carbon Nanotubes (MWCNTs) as stationary phase packed columns for the gas chromatographic separation of alkanes and aromatic hydrocarbons and Surface properties were verified by inverse gas chromatography. The results showed the separation of the n-alkanes (C3–C5) and aromatic alkanes [57]. The typical stationary phases are derivatives from silica, carbon, alumina, polymer, or minerals. The carbon-based materials are very stable and have porosity suitable to be applied as a column stationary phase [36,58,59].

Therefore, this work aimed to apply various starting materials such as Chitosan or 4-Amino-3-hydroxy-napthalene-1-sulphnic acid for Schiff's base modification process to fabricate covalent organic layer/carbon hybrid materials. Characterize with TEM, XRD, FTIR, and surface area, in addition, to applying inverse gas chromatography to assess the surface free energy and thermodynamic properties of the fabricated materials during the separation of hydrocarbon mixtures.

2. Experimental

2.1. Reagents and Materials

Silica capillaries with an inner diameter of 250 µm were purchased from Restek (Bellefonte, PA, USA). High-purity gases (99.9999%) (air, helium, hydrogen, nitrogen, and methane) were obtained from SIGAS (Riyadh, Saudi Arabia). n-alkanes (pentane, hexane, heptane, octane, nonane, decane, undecane, and dodecane), Chitosan, ethanol, Acetic acid, 4-(Dimethyl amino) benzaldehyde, 4-(Dimethyl amino)benzaldehyde were purchased from sigma. Carbon materials were provided by Dr. Habila's group as prepared previously [60].

2.2. Fabrication of Functioned Carbon Materials via Schiff's Base Process

Two Schiff's base processes were applied to fabricate carbon coated with Chitosan-derived covalent organic layer (C@Chitosan-COL) as well as Schiff's base derived sulfonated carbon (Schiff's-C-S). For the fabrication of C@Chitosan-COL, a mass of 1.5 g of

Chitosan was dissolved in a mixture of 200 mL ethanol and 50 mL acetic acid. Then, 1.49 g of 4-(Dimethyl amino) benzaldehyde was added, and the solution was ultrasonicated for 15 min. The mixture was maintained at 25 °C under stirring for 24 h. Next, the solution was centrifuged at 6000 rpm for 10 min, and the precipitate was dispersed in ethanol and impregnated with carbon in ethanol medium, then treated under autoclave oven conditions at 120 °C for 12 h.

A mass of 2.39 g of 4-Amino-3-hydroxy-napthalene-1-sulphnic acid was dissolved in 200 mL ethanol to fabricate Schiff's-C-S. To this solution, 1.49 g of 4-(Dimethyl amino) benzaldehyde was added, and the solution was ultra-sonicated for 15 min. The mixture was then maintained at 25 °C under stirring for 24 h. The solution was centrifuged at 6000 rpm for 10 min, and the precipitate was washed several times with water and ethanol. The obtained product was placed in a drying oven at 120 °C for 12 h, followed by one step carbonization–activation at 300 °C to produce.

2.3. Instrumentation

All GC separations were performed on a conventional gas chromatograph, Shimadzu 2025 Series (Kyoto, Japan) with a split/splitless injector, a column oven with a temperature range of 323–673 K, and a flame ionization detector (FID). The temperature range for all the experiments was 303–353 K, under a pressure of 30 kPa for the C@Chitosan-COL column and 250 kPa for Schiff's-C-S column. The detector and injector were set at 523 K, and the carrier gas was ultrapure helium.

A spectrometer (Nicolet 6700, Thermo Scientific, Madison, WI, USA) was used to record the infrared spectra (FTIR). X-ray diffraction (XRD) was obtained using MiniFlex-600, Rigaku (Tokyo, Japan) with Cu Ka irradiation. A transition electron microscope (TEM) was used to shape and structure the formed materials.

2.4. Capillary Coating

All columns were prepared using a fused silica capillary 15 m long and an inner diameter of 250 μm. The silica inner surface of the capillaries was first treated with 1.0 M sodium hydroxide solution for 120 min under a flow rate of 40 μL min^{-1}, then washed thoroughly with water for 30 min. The procedure was repeated with 0.1 M hydrochloric acid solution, then flushed thoroughly with water until neutral. Finally, the column was dried under a stream of nitrogen at 423 K for 24 h.

After this surface activation, the prepared materials were coated onto the inner walls of the capillaries by a dynamic coating method [61]. Briefly, 1 mL of 5% ethanol suspension was filled into the capillary column and then pushed out at 40 cm min^{-1} to form a thin coated layer on the inner wall. A 1 m buffer capillary restrictor was added to the column end to prevent solution acceleration. The capillary columns were conditioned after coating under nitrogen for two hours, then under a GC temperature program of 303 K for 15 min, ramping to 573 K with a ramp rate of 3 K min^{-1}, then treated at 573 K for one hour, the temperature program was triplicated. The precise weight of the coated material was estimated through empty to the coated capillary weight difference.

2.5. Chromatographic Evaluation

Selectivity (α) represents the chromatographic system's capability to distinguish different analytes and is determined as the rate of the reduced retention times [62]:

$$\alpha = \frac{k_2}{k_1} = \frac{t_{R2} - t_m}{t_{R1} - t_m} \quad (1)$$

where t_R is the retention time, and t_m is the dead time estimated experimentally using methane gas as an unretained material.

Resolution (R_S) as the degree of separation between neighboring solute bands or peaks was calculated using Equation (2) [63].

$$R_S = 1.18 \frac{t_{R2} - t_{R1}}{w_{(1/2)1} + w_{(1/2)2}} \quad (2)$$

where $w_{(1/2)}$ is the peak width at half height.

2.6. Thermodynamic Calculations

Adsorption properties indicated by surface thermodynamic parameters were determined by inverse gas chromatography (IGC) [64].

All thermodynamic parameters were derived from The retention volume:

$$V_N = (t_R - t_M)\, F_a \frac{T}{T_a} J \quad (3)$$

where F_a is the volumetric flow rate ($cm^3\ min^{-1}$), T and T_a are the column temperature and the ambient temperature (K), respectively, and J is the James–Martin gas compressibility Correction factor calculated by the following equation:

$$J = \frac{(3P^2 - 1)}{(2P^3 - 1)} \quad (4)$$

With P being P_i/P_o, P_i is the column inlet pressure, and P_o is the column outlet pressure [65].

The free energy of adsorption, ΔG_A, is related to V_N by equation (5):

$$\Delta G_A = -RT\ln \frac{V_N P^0}{S\pi_0} \quad (5)$$

where R is the ideal gas constant, S is the specific surface area of the adsorbent, π_0 is the reference two-dimensional surface pressure, and P^o is the adsorbate vapor pressure in the standard gaseous state, which is calculated from Antoine's equation:

$$\mathrm{Log}\,(P^0) = A - \left(\frac{B}{t + C}\right) \quad (6)$$

A, B, and C are the Antoine coefficients [66], and t is the column temperature in Celsius [67].

The enthalpy of adsorption, ΔH_A, the slope of linear relation of $\ln V_N$ versus 1/T

$$\Delta H_A = -R\frac{d\ \ln VN}{d(1/T)} \quad (7)$$

The entropy of adsorption, ΔS_A, is evaluated from ΔG_A and ΔH_A values [68]:

$$\Delta S_A = \frac{\Delta H_A - \Delta G_A}{T} \quad (8)$$

The dispersive component of surface energy (γ_S^D) demonstrate the Van der Waals forces tendency of an adsorbent surface, equivalent to surface tension in liquids [69]. Schultz et al. method [70] is the primary method to estimate adsorbate–adsorbent dispersive interactions. The dispersive component of surface energy estimated by the Schultz et al. method from the slope of the relation between RT $\ln V_N$ against a $(\gamma_L^D)^{1/2}$ of a linear alkanes series, where γ_L^D is the dispersive free energy of the probe (Table 1), according to Equation (9).

$$RT\ \ln V_N = 2\,N\,a\,\sqrt{\gamma_L^D \cdot \gamma_S^D} + K \quad (9)$$

where N is Avogadro's number, and a is the cross-sectional area of the probe.

Table 1. Characteristics for selected n-alkanes solvents (nonane, decane, undecane, dodecane).

Probe	a (Å^2)	γ_L^D (mJ m^{-2})	a $(\gamma_L^D)^{1/2}$ (m^2 kJ$^{-1/2}$ m^{-1})
n-nonane	69	22.7	3.29×10^{-21}
n-decane	75	23.4	3.63×10^{-21}
n-undecane	81	24.6	4.01×10^{-21}
n-dodecane	87	25.4	4.38×10^{-21}

3. Results and Discussion

3.1. Characterization of the Fabricated Functioned Carbon Materials

The prepared carbon coated with Chitosan-derived covalent organic layer (C@Chitosan-COL) as well as Schiff's base derived sulfonated carbon (Schiff's-C-S) is examined with TEM, FTIR, and XRD to assess their particles shapes, dimensions, crystallinity, surface functional groups, and layers. In Figures 1 and 2, the amorphous structure is dominant for the two formed materials due to the formation of a carbon skeleton with surface functional groups at the end.

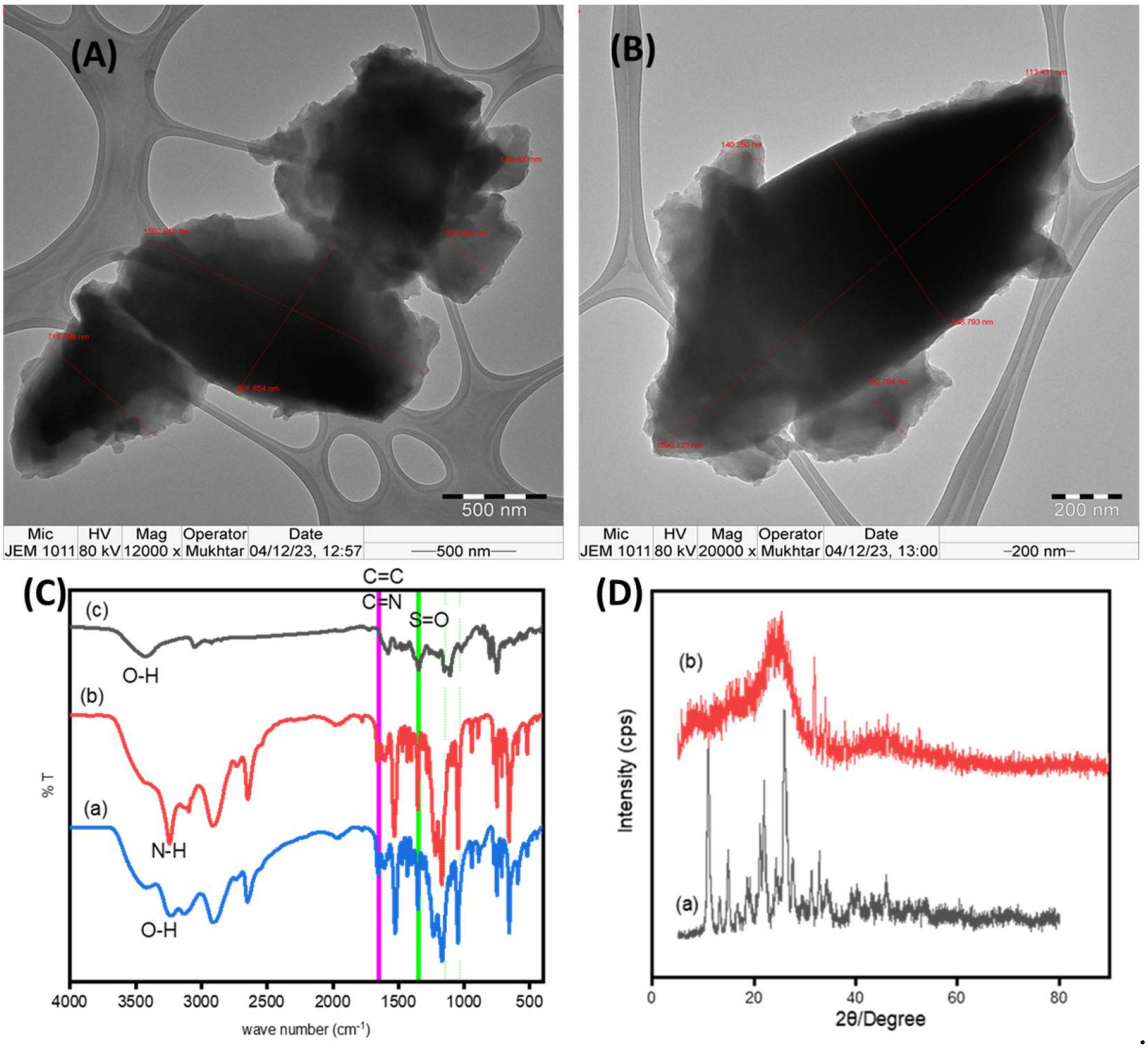


Figure 1. TEM of Schiff's-C-S at a magnification of (**A**) 12,000 and (**B**) 20,000. (**C**)The FTIR spectrum ((a) Schiff's base, (b) 4-amino-3-hydroxy-naphthalene-1-sulphonic acid, (c) Schiff's-C-S). (**D**) XRD spectrum ((a) Schiff's base and (b) Schiff's-C-S).

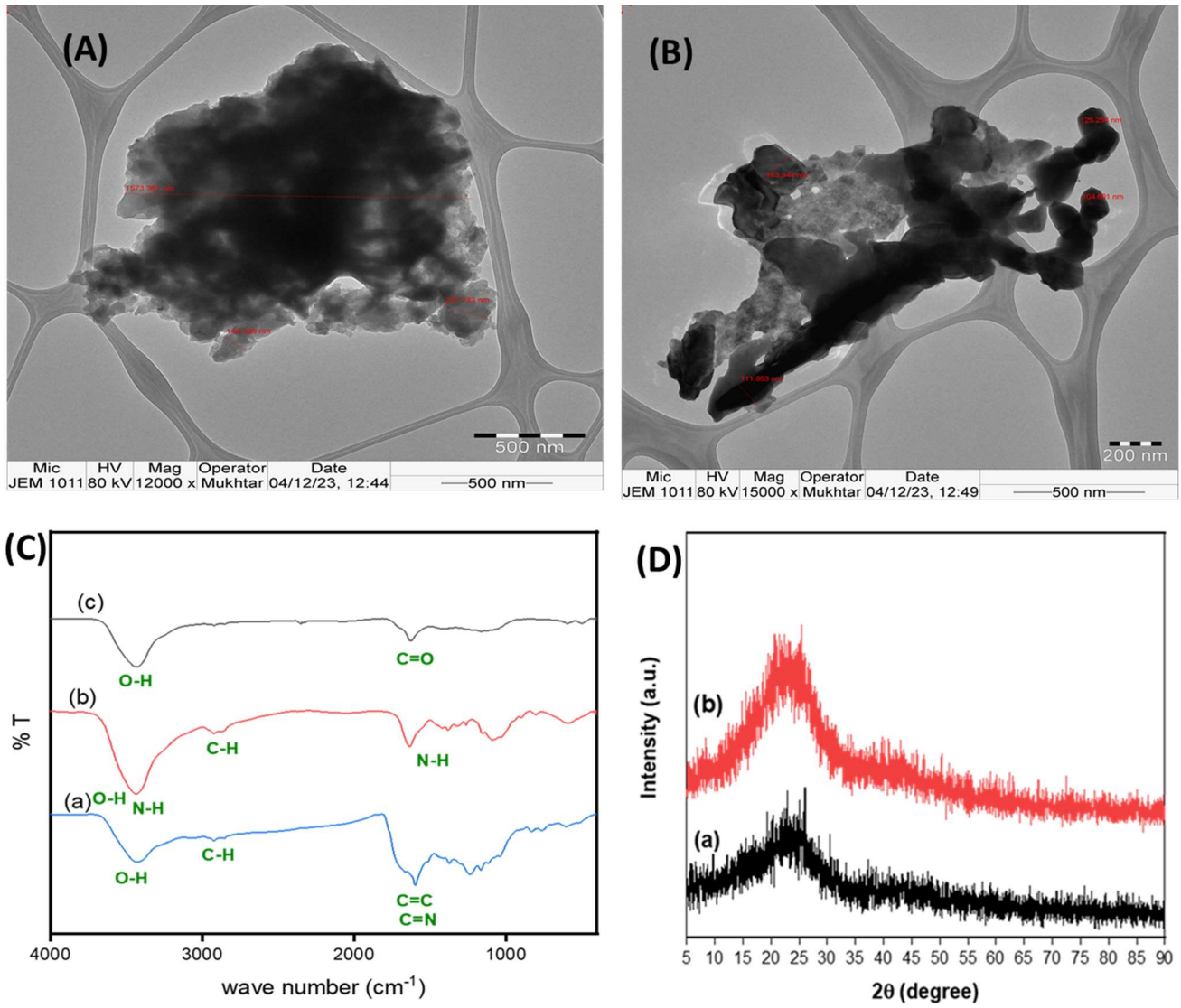


Figure 2. TEM of C@Chitosan-COL at magnification (**A**) 12,000 and (**B**) 15,000. (**C**) The FTIR spectrum ((a) C@Chitosan-COL, (b) chitosan, (c) carbon). (**D**) XRD spectrum ((a) carbon and (b) C@Chitosan-COL).

The Schiff's-C-S is formed in a convex particle shape with dimensions between 600 nm and 1500 nm. These particles contain side buildings with dimensions between 140 nm and 316 nm, as shown in Figure 1A,B. The FTIR spectrum of the 4-Amino-3-hydroxy-napthalene-1-sulphnic acid derived Schiff base and their derived carbon (Schiff's-C-S) produced by carbonization at 300 °C was shown in Figure 1C. The FTIR spectrum for 4-Amino-3-hydroxy-napthalene-1-sulphnic acid shows characteristic absorption bands at 2743, 2907, 1659, and 1594 cm^{-1} was associated with stretching vibrations of ν(C–H) aldehyde, ν(C–H) methyl group, ν(C–H) benzene, ν(C=O), and ν(C=C) group, respectively (Figure 1C(b). The formed Schiff's base materials show a characteristic stretching absorption peak at 1651 cm^{-1} due to forming a new bond for ν(C=N) (Figure 1C(a)), indicating the successful formation of the Schiff's base by reaction of 4-dimethylamino benzaldehyde with 4-amino-3-hydroxy-naphthalene-1-sulphonic acid [71]. The peaks at 3238, 3442, 3125, and 1606 cm^{-1} assigned to υ(OH) group, ν(C=C) aromatic, ν(C-H) methyl, ν(C=C) aromatic, respectively. After the hydrothermal carbonization of Schiff's-C-S at 300 °C, it's clear that the broad-band at 3413 cm^{-1} was attributed to the O-H group. The stretching absorption peak at 1651 cm^{-1} is due to forming a new bond for ν(C=N). The S=O group is detected at around 1350–1400 cm^{-1} (Figure 1C(c) [21]. The reaction of 4-dimethylamino benzaldehyde with

4-amino-3-hydroxy-naphthalene-1-sulphonic acid resulted in the formation of crystalline materials as indicated from XRD peaks (Figure 1D(a)). In contrast, the peaks are reduced and shielded after carbonization due to forming a carbonaceous structure (Schiff's-C-S). The porosity examination showed a BET surface area of 9.2531 m^2/g, Langmuir surface area of 11.5796 m^2/g, and average pore width of 17.9217 Å.

The C@Chitosan-COL is formed in two layers of activated carbon which is covered by Chitosan-based covalent organic layer-derived carbon with particle sizes about 1573 nm, which exhibit side extensions with dimensions between 100 nm and 227 nm, as shown in Figure 2A,B. The FTIR spectrum is presented in Figure 2C, where the FTIR spectra of pure Chitosan. Figure 2C(b) showed peaks related to stretching vibrations of υ(O-H/N-H)), C-H, and bending vibration of N-H of primary amine at 3400, 2900, and 1590 $cm^{-1,}$ respectively [72]. In contrast, the carbon (Figure 2C(c)) exhibited a band for O-H at 3400 and C=O at about 1650 cm^{-1} [73]. The C@Chitosan-COL (Figure 2C(a)) exhibited the two characteristic bands at 3432 and 1631 cm^{-1} were attributed to the stretching vibrations of υ(O-H) and ν(C=N/C=C) bonds, respectively [74]. It seems the combined bands between 1600 and 1700 to be an envelope of many double bond related bands related to C=C, C=N, and C=O, in addition to the protonated amine groups as well as amine, acetamide and/or imine groups have been reported to absorb in this region [73,75,76]. The XRD patterns of the carbon (Figure 2D(a)) and C@Chitosan-COL (Figure 2D(b)) showed the two characteristic diffraction peaks at 2θ = 22.89° and 43.34° corresponded well to the semicrystalline structure of carbon [77]. Upon performing surface modification of activated carbon (C@Chitosan-COL) did not show any noticeable changes at the peaks, suggesting the maintenance of activated carbon's semicrystalline nature. The porosity examination showed a BET surface area of 21.0854 m^2/g, Langmuir surface area of 29.0986 m^2/g, and average pore width of 13.5595 Å.

3.2. Chromatographic Evaluation

For this purpose, this paper collected Schiff's base and carbon materials and used them as a stationary phase in gas chromatography, giving the best efficiency for separating some hydrocarbons. Column C@Chitosan-COL successfully separated a series of hydrocarbons (nonane, decane, and undecane) at a pressure of 30 kPa and an isothermal temperature of 333 K (Figure 3). The selectivity values of nonane/decane and decane/undecane pairs were 1.34 and 1.64, respectively. A resolution > 1.18 indicated complete separation for the selected probes. Column Schiff's-C-S separated nonane, decane, undecane, and dodecane, with a selectivity ranging from 1.36 to 1.92 and a resolution in the range 0.3–1.3 (Figure 4), under a pressure of 250 kPa and a constant temperature of 333 K. The presence of surface functional groups such as C-H, C=C, C=N, and S=O enhances the column performance for the separation of hydrocarbon using the fabricated columns due to the gradual interaction between alkanes carbon chains and surface functional groups, producing a well-separated peak. This interaction could be owed to the van der Waals forces between the hydrocarbon mixture and surface functional groups of C@Chitosan-COL and Schiff's-C-S which mainly depend on the chain length creating a variation in the interaction degree and allow the low molecular weight to exit from the capillary chromatographic column first and the highest molecular weight to exit later with suitable retention time enough to obtain separated peaks (Figures 3 and 4). There are no positive separation results in the case of using an empty capillary column or without modification. Thus, we keep and report the achievements as well as the meaningful results to indicate the effectiveness of the fabricated materials, including C@Chitosan-COL and Schiff's-C-S for hydrocarbon separation. The prepared capillary column for gas chromatographic separations using the fabricated materials are reused several times during this study for the separation of hydrocarbon mixtures. The activation process is just to raise the temperature to 523 K between each use.

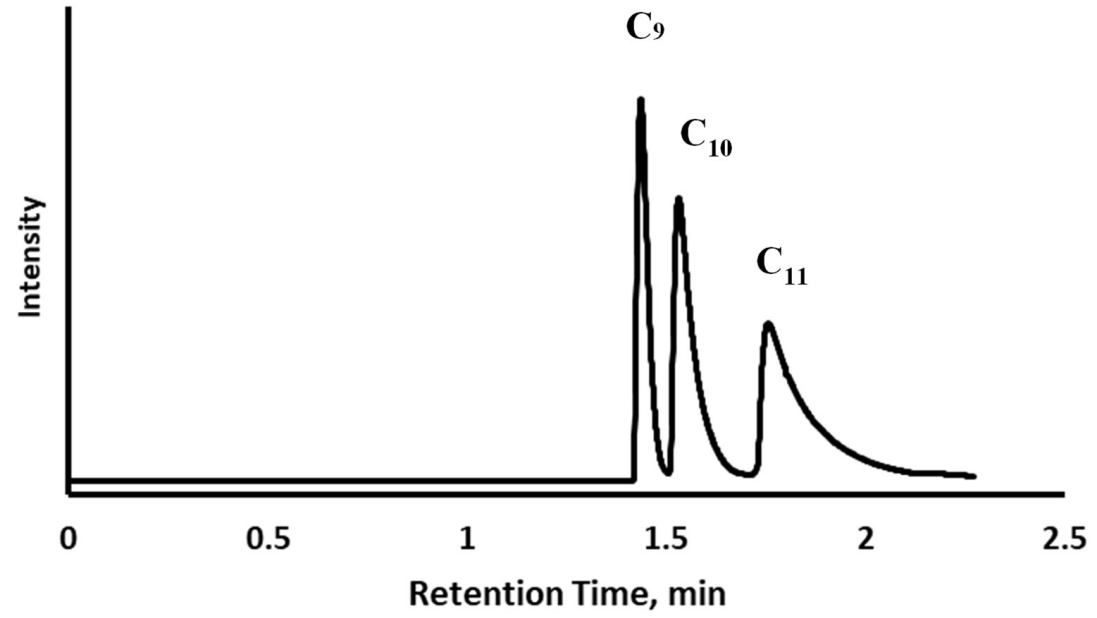


Figure 3. Chromatogram of a nonane, decane, and undecane separation on column C@Chitosan-COL at 333 K and 30 kPa.

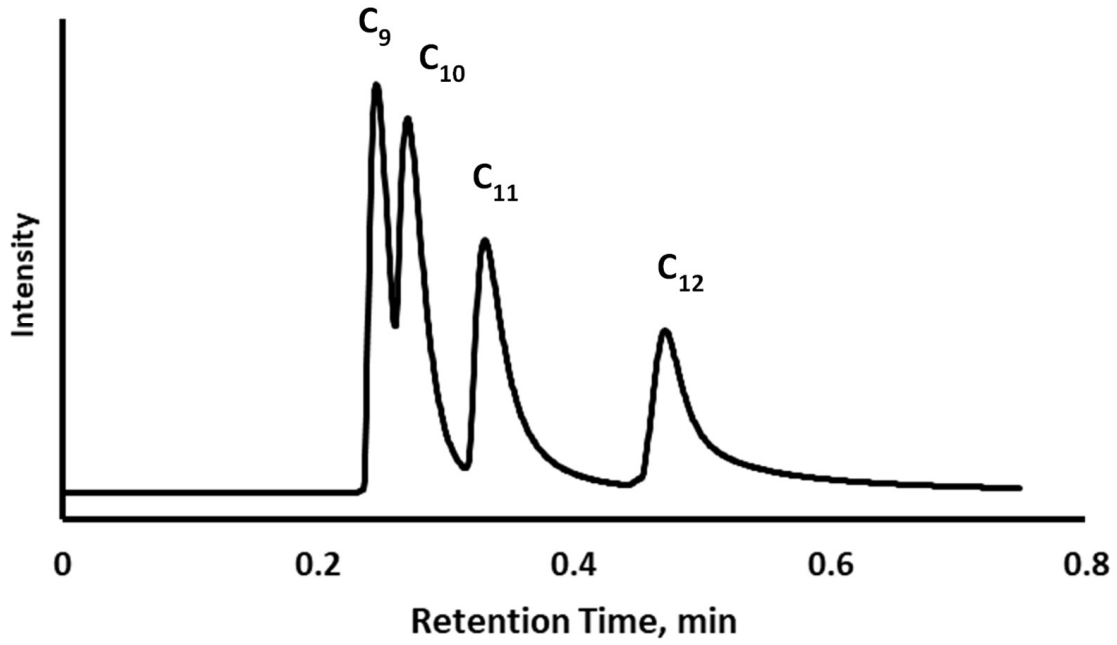


Figure 4. Chromatogram of a nonane, decane, undecane, and dodecane separation on column Schiff's-C-S at 333 K and 250 kPa.

3.3. Thermodynamic Parameters Calculations

Physicochemical properties of alkane series adsorption over the studied Schiff's bases were estimated using an inverse gas chromatography approach over a temperature range of 313–343 K. Van't Hoff plots showed a linear relationship between the reversed absolute temperature and the normal logarithm of Henry's constant, demonstrating a homogeneous separation mechanism throughout the surface of the adsorbents (Figure 5A,B) [78].

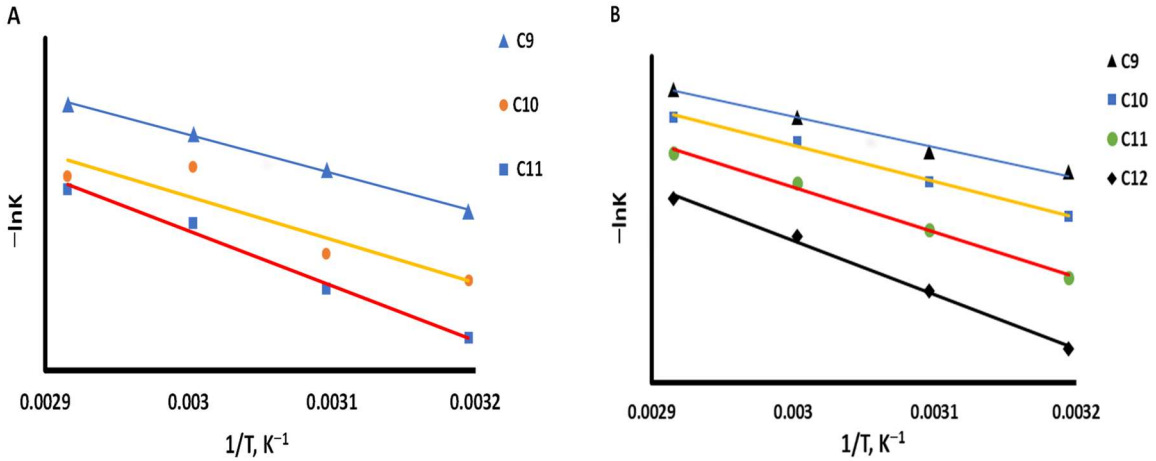


Figure 5. Van't Hoff plots at 313–343 K for (**A**) nonane, decane, and undecane on C@Chitosan-COL at 30 kPa, and (**B**) nonane, decane, undecane, and dodecane on Schiff's-C-S at 250 kPa.

The value of free energy change for adsorption (ΔG_A) is determined by adding up the adsorption energies resulting from dispersive and specific interactions. As per research, when n-alkanes are used as nonpolar probes, their adsorption occurs solely through dispersive interactions [79]. The negative values of ΔG_A indicate a spontaneous transfer of solutes from the mobile phase to the stationary phase for C@Chitosan-COL and Schiff's-C-S under the studied temperature range (313–343 K) (Table 2). Notably, the free energy change of adsorption values of Schiff's-C-S surpassed those of C@Chitosan-COL, indicating higher adsorption density.

Table 2. Gibbs free energy of adsorption (ΔG_A) values at 313–343 K for nonane, decane, and undecane on C@Chitosan-COL, and nonane, decane, undecane, and dodecane on Schiff's-C-S.

Probe	$-\Delta G_A$ (kJ mol^{-1})							
	C@Chitosan-COL				Schiff's-C-S			
	313 K	323 K	333 K	343 K	313 K	323 K	333 K	343 K
n-Nonane	6.49	7.20	7.94	8.78	9.68	10.80	11.38	12.09
n-Decane	5.42	6.59	6.18	8.09	8.40	9.20	9.65	10.57
n-Undecane	3.69	4.45	4.68	5.63	7.26	7.79	8.18	9.06
n-Dodecane	-	-	-	-	7.05	7.31	7.56	8.25

Physical adsorption was indicated by the enthalpy of adsorption values less than 62.8 kJ/mol, which is the borderline between chemical and physical adsorption (Table 3) [67]. Furthermore, the results show an increase in the enthalpy value with the increase in the number of carbon atoms, consistent with previous studies (Table 3) [80].

Table 3. Entropy change of adsorption (ΔH_A) values at 313–343 K for nonane, decane, and undecane on C@Chitosan-COL, and nonane, decane, undecane, and dodecane on Schiff's-C-S.

Probe	$-\Delta H_A$ (kJ mol^{-1})	
	C@Chitosan-COL	Schiff's-C-S
	313–343 K	313–343 K
n-Nonane	25.80	28.33
n-Decane	29.35	34.04
n-Undecane	38.58	42.99
n-Dodecane	-	52.73

A proportional linear relationship between hydrocarbon chain length and change in enthalpy was observed due to the additive nature of dispersive interaction (Figure 6) [81].

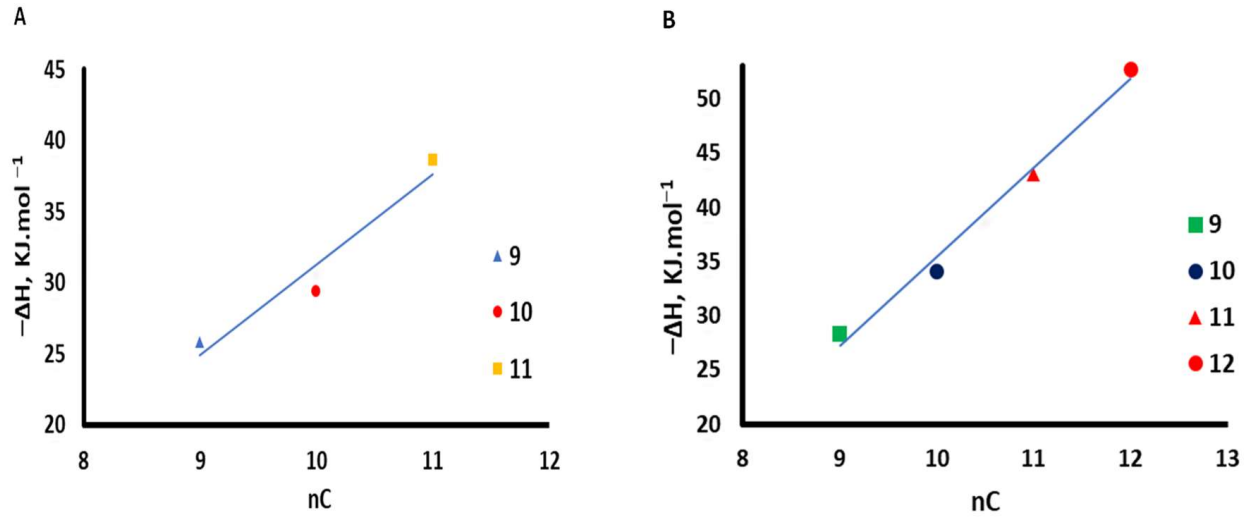


Figure 6. Effects of the alkyl chain length on the enthalpy of adsorption (ΔH_A) at 313–343 K for (**A**) nonane, decane, and undecane on C@Chitosan-COL at 30 kPa, and (**B**) nonane, decane, undecane, and dodecane on Schiff's-C-S at 250 kPa.

The entropy changes of adsorption (ΔS_A) increased with increasing chain length demonstrating less random movement and higher adsorption in both materials (Table 4). As expected, an increase in the system's randomness was detected with increasing temperature, indicated by decreasing the entropy of adsorption values (Table 4).

Table 4. Entropy change of adsorption (ΔS_A) values at 313–343 K for nonane, decane, and undecane on C@Chitosan-COL, and nonane, decane, undecane, and dodecane on Schiff's-C-S.

Probe	$-\Delta S_A$ (J mol^{-1} K^{-1})							
	C@Chitosan-COL				Schiff's-C-S			
	313 K	323 K	333 K	343 K	313 K	323 K	333 K	343 K
n-Nonane	61.69	57.59	53.63	49.63	59.54	54.24	50.88	47.31
n-Decane	76.43	70.44	69.58	61.97	81.88	76.88	73.21	68.39
n-Undecane	111.47	105.68	101.79	96.07	114.14	108.97	133.79	98.92
n-Dodecane	-	-	-	-	145.94	140.61	135.65	129.68

The Schultz et al. method was used to determine the dispersive component of surface energy γ_s^d, which is an indication of solid surface activity [70]. Figure 7 shows the linear relation between RT lnV_N versus a $(\gamma_L^D)^{1/2}$ values at 313–343 K correspond to the dispersive interactions of the linear alkanes sample. The calculated values from the slope of the proposed relation were lower than the literature values of similar materials, possibly due to the large pores within the structure of the studied Schiff's bases. γ_s^d values decreased with increasing temperature (Table 5), inconsistent with previous studies [82].

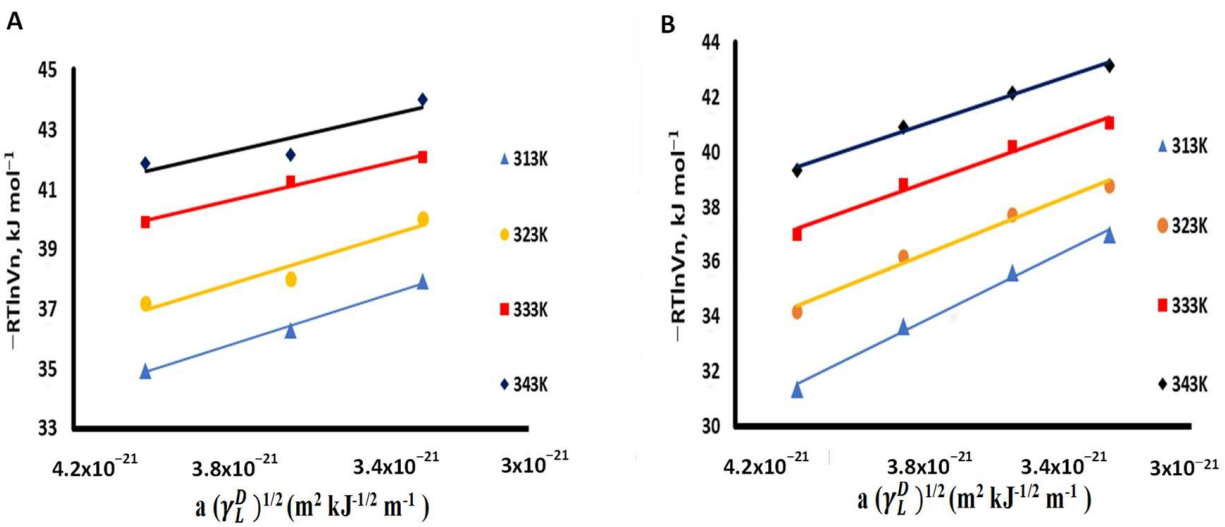


Figure 7. Free energy of adsorption (RT $\ln V_N$) as a function of the descriptor a $(\gamma_L^D)^{1/2}$ to estimate the specific interaction according to Schultz et al. approach at 313–343 K for (**A**) nonane, decane, and undecane on C@Chitosan-COL at 30 kPa, and (**B**) nonane, decane, undecane, and dodecane on Schiff's-C-S at 250 kPa.

Table 5. The dispersive component of surface energy γ_S^D values using the Schultz et al. method for C@Chitosan-COL and Schiff's-C-S at 313–343 K range.

T (K)	γ_S^D (mJ m^{-2})	
	C@Chitosan-COL	Schiff's-C-S
313	11.41	18.206
323	10.41	12.071
333	6.26	9.410
343	-	8.40

4. Conclusions

Carbon functioned structures, including carbon coated with Chitosan-derived covalent organic layer (C@Chitosan-COL) as well as Schiff's base-derived sulfonated carbon (Schiff's-C-S), were developed via a combination of Schiff's base with thermal treatment processes. The carbon materials developed in this work exhibited surface functional groups with heteroatoms such as O-H, C=N, and S=O, which provide the surface electronic environment suitable for the separation of hydrocarbon mixture including n-Nonane, n-Decane, n-Undecane, n-Dodecane. The thermodynamic parameters indicated spontaneous adsorption, which enhance the hydrocarbon separation. Physical adsorption was suggested by the enthalpy of adsorption values less than 62.8 kJ/mol, which is the borderline between chemical and physical adsorption. The obtained results of hydrocarbon separation indicated the potential of the developed C@Chitosan-COL and Schiff's-C-S for further future applications as stationary phase in chromatographic applications for separating various mixtures and pollutants. Combining Schiff's base with thermal treatment as a process for developing carbon with specific functionalization id still opens space to enhance future research for materials devilments for separation and chromatographic applications.

Author Contributions: Conceptualization, M.A.H.; formal analysis, A.S.A., K.Y. and M.A.H.; funding acquisition, Z.A.A.; investigation, A.S.A.; methodology, K.Y., M.A.H. and Z.A.A.; resources, Z.A.A.; validation, A.S.A., K.Y. and M.A.H.; writing—original draft, A.S.A., K.Y. and M.A.H.; writing—review and editing, K.Y. and M.A.H. All authors have read and agreed to the published version of the manuscript.

Funding: This work was funded by the Deputyship for Research & Innovation, Ministry of Education in Saudi Arabia.

Institutional Review Board Statement: Not applicable.

Informed Consent Statement: Not applicable.

Data Availability Statement: Samples of the compounds are available from the authors.

Acknowledgments: The authors extend their appreciation to the Deputyship for Research & Innovation, Ministry of Education in Saudi Arabia for funding this research. (IFKSURC-1-3302).

Conflicts of Interest: The authors declare no conflict of interest.

References

1. Fang, Y.X.; Lin, Y.F.; Xu, Z.L.; Mo, J.W.; Li, P.P. A Novel Clover-like COFs Membrane Fabricated via One-Step Interfacial Polymerization for Dye/Salt Separation. *J. Membr. Sci.* **2023**, *673*, 121470. [CrossRef]
2. Li, Z.; Zheng, Y.; Gu, T.; Meng, X.; Wang, H.; Xu, K.; Cheng, L.; Kasher, R.; Zhang, R.; Jiang, Z. Covalent Organic Framework Membrane with Sub-Nano Pores for Efficient Desalination. *J. Membr. Sci.* **2023**, *675*, 121551. [CrossRef]
3. Ma, D.; Ma, D.; Li, Z.; Zhu, J.; Zhou, Y.; Chen, L.; Mai, X.; Liufu, M.; Wu, Y.; Li, Y. Inverse and Highly Selective Separation of CO2/C2H2 on a Thulium–Organic Framework. *J. Mater. Chem. A Mater.* **2020**, *8*, 11933–11937. [CrossRef]
4. Atanes, E.; Cuesta-García, B.; Nieto-Márquez, A.; Fernández-Martínez, F. A Mixed Separation-Immobilization Method for Soluble Salts Removal and Stabilization of Heavy Metals in Municipal Solid Waste Incineration Fly Ash. *J. Environ. Manag.* **2019**, *240*, 359–367. [CrossRef]
5. Kumar, P.; Guliants, V.V. Periodic Mesoporous Organic–Inorganic Hybrid Materials: Applications in Membrane Separations and Adsorption. *Microporous Mesoporous Mater.* **2010**, *132*, 1–14. [CrossRef]
6. Krukonis, V.J. *Supercritical Fluid Extraction in Flavor Applications*; ACS: Washington, DC, USA, 1985; pp. 154–175. [CrossRef]
7. Camel, V. Solid Phase Extraction of Trace Elements. *Spectrochim. Acta* **2003**, *58*, 1177–1233. [CrossRef]
8. Shyam Sunder, G.S.; Adhikari, S.; Rohanifar, A.; Poudel, A.; Kirchhoff, J.R. Evolution of Environmentally Friendly Strategies for Metal Extraction. *Separations* **2020**, *7*, 4. [CrossRef]
9. ALOthman, Z.A.; Wabaidur, S.M. Application of Carbon Nanotubes in Extraction and Chromatographic Analysis: A Review. *Arab. J. Chem.* **2019**, *12*, 633–651. [CrossRef]
10. Ruthven, D.M. *Principles of Adsorption and Adsorption Processes*; John Wiley & Sons: Hoboken, NJ, USA, 1984; ISBN 0471866067.
11. Cooney, D.O. *Adsorption Design for Wastewater Treatment*; CRC Press: Boca Raton, FL, USA, 1998; ISBN 1566703336.
12. Antony, R.; Arun, T.; Manickam, S.T.D. A Review on Applications of Chitosan-Based Schiff Bases. *Int. J. Biol. Macromol.* **2019**, *129*, 615–633. [CrossRef] [PubMed]
13. Monier, M.; Ayad, D.M.; Abdel-Latif, D.A. Adsorption of Cu(II), Cd(II) and Ni(II) Ions by Cross-Linked Magnetic Chitosan-2-Aminopyridine Glyoxal Schiff's Base. *Colloids Surf. B Biointerfaces* **2012**, *94*, 250–258. [CrossRef]
14. Tsaneva, D.; Nikolova, M.; Prokopov, T.; Petkova, N.; Stoyanova, A.; Denev, P. Evaluation of Adsorption Capacity of Chitosan-Cinnamaldehyde Schiff Base. *J. Pharm. Sci. Res.* **2017**, *9*, 1609.
15. Wang, Y.; Liu, W.; Zhang, J.; Shan, Q. Preparation of Co-Schiff Base Complex and Its Adsorption Desulfurization. *Fuel* **2022**, *324*, 124696. [CrossRef]
16. Xu, G.; Hou, L.; Li, B.; Wang, X.; Liu, L.; Li, N.; Wang, M.L.; Zhao, R.S. Facile Preparation of Hydroxyl Bearing Covalent Organic Frameworks for Analysis of Phenoxy Carboxylic Acid Pesticide Residue in Plant-Derived Food. *Food Chem.* **2021**, *345*, 128749. [CrossRef]
17. Segura, J.L.; Mancheño, M.J.; Zamora, F. Covalent Organic Frameworks Based on Schiff-Base Chemistry: Synthesis, Properties and Potential Applications. *Chem. Soc. Rev.* **2016**, *45*, 5635–5671. [CrossRef]
18. Qian, C.; Qi, Q.Y.; Jiang, G.F.; Cui, F.Z.; Tian, Y.; Zhao, X. Toward Covalent Organic Frameworks Bearing Three Different Kinds of Pores: The Strategy for Construction and COF-to-COF Transformation via Heterogeneous Linker Exchange. *J. Am. Chem. Soc.* **2017**, *139*, 6736–6743. [CrossRef]
19. Yang, Z.; Sun, P. Compare of Three Ways of Synthesis of Simple Schiff Base. *Molbank* **2006**, *2006*, M514. [CrossRef]
20. Bhat, A.R.; Wagay, M.H. Synthesis of Schiff's Base Derivatives Using Water as Solvent. (A Green Methodology). *Int. J. Res. Appl. Sci. Eng. Technol.* **2017**, *5*, 971–982. [CrossRef]
21. Li, W.; Wang, Q.; Cui, F.; Jiang, G. Covalent Organic Framework with Sulfonic Acid Functional Groups for Visible Light-Driven CO_2 Reduction. *RSC Adv.* **2022**, *12*, 17984–17989. [CrossRef]
22. Peng, Y.; Xu, G.; Hu, Z.; Cheng, Y.; Chi, C.; Yuan, D.; Cheng, H.; Zhao, D. Mechanoassisted Synthesis of Sulfonated Covalent Organic Frameworks with High Intrinsic Proton Conductivity. *ACS Appl. Mater. Interfaces* **2016**, *8*, 18505–18512. [CrossRef] [PubMed]
23. Li, F.; Ding, L.G.; Yao, B.J.; Huang, N.; Li, J.T.; Fu, Q.J.; Dong, Y. Bin Pd Loaded and Covalent-Organic Framework Involved Chitosan Aerogels and Their Application for Continuous Flow-through Aqueous CB Decontamination. *J. Mater. Chem. A Mater.* **2018**, *6*, 11140–11146. [CrossRef]

24. Fontana, R.; Marconi, P.C.R.; Caputo, A.; Gavalyan, V.B. Novel Chitosan-Based Schiff Base Compounds: Chemical Characterization and Antimicrobial Activity. *Molecules* **2022**, *27*, 2740. [CrossRef] [PubMed]
25. Cavallaro, G.; Micciulla, S.; Chiappisi, L.; Lazzara, G. Chitosan-Based Smart Hybrid Materials: A Physico-Chemical Perspective. *J. Mater. Chem. B* **2021**, *9*, 594–611. [CrossRef] [PubMed]
26. Li, X.; Zhou, H.; Wu, W.; Wei, S.; Xu, Y.; Kuang, Y. Studies of Heavy Metal Ion Adsorption on Chitosan/Sulfydryl-Functionalized Graphene Oxide Composites. *J. Colloid Interface Sci.* **2015**, *448*, 389–397. [CrossRef]
27. Garcia Peña, L.V.; Petkova, P.; Margalef-Marti, R.; Vives, M.; Aguilar, L.; Gallegos, A.; Francesko, A.; Perelshtein, I.; Gedanken, A.; Mendoza, E.; et al. Hybrid Chitosan-Silver Nanoparticles Enzymatically Embedded on Cork Filter Material for Water Disinfection. *Ind. Eng. Chem. Res.* **2017**, *56*, 3599–3606. [CrossRef]
28. Pratibha; Kapoor, A.; Rajput, J.K. Electroactive Core-Shell Chitosan-Coated Lanthanum Iron Oxide as a Food Freshness Level Indicator for Tyramine Content Determination. *ACS Sustain. Chem. Eng.* **2022**, *10*, 11666–11679. [CrossRef]
29. Mohd Adnan, M.A.; Bao, L.P.; Muhd Julkapli, N. Mitigation of Pollutants by Chitosan/Metallic Oxide Photocatalyst: A Review. *J. Clean Prod.* **2020**, *261*, 121190. [CrossRef]
30. Li, W.; Jiang, H.X.; Geng, Y.; Wang, X.H.; Gao, R.Z.; Tang, A.N.; Kong, D.M. Facile Removal of Phytochromes and Efficient Recovery of Pesticides Using Heteropore Covalent Organic Framework-Based Magnetic Nanospheres and Electrospun Films. *ACS Appl. Mater. Interfaces* **2020**, *12*, 20922–20932. [CrossRef] [PubMed]
31. Wang, Z.; Zhang, S.; Chen, Y.; Zhang, Z.; Ma, S. Covalent Organic Frameworks for Separation Applications. *Chem. Soc. Rev.* **2020**, *49*, 708–735. [CrossRef]
32. Yuan, S.; Li, X.; Zhu, J.; Zhang, G.; Van Puyvelde, P.; Van Der Bruggen, B. Covalent Organic Frameworks for Membrane Separation. *Chem. Soc. Rev.* **2019**, *48*, 2665–2681. [CrossRef]
33. Xie, M.; Quan, K.; Li, H.; Liu, B.; Chen, J.; Yu, Y.; Wang, J.; Qiu, H. Non-Porous Silica Support Covalent Organic Frameworks as Stationary Phases for Liquid Chromatography. *Chem. Commun.* **2023**, *59*, 314–317. [CrossRef]
34. Yusuf, K.; Natraj, A.; Li, K.; Ateia, M.; ALOthman, Z.A.; Dichtel, W.R. Inverse Gas Chromatography Demonstrates the Crystallinity-Dependent Physicochemical Properties of Two-Dimensional Covalent Organic Framework Stationary Phases. *Chem. Mater.* **2023**, *35*, 1691–1701. [CrossRef]
35. Zheng, Y.; Wan, M.; Zhou, J.; Dai, X.; Yang, H.; Xia, Z.; Wang, L. One-Pot Method for the Synthesis of β-Cyclodextrin and Covalent Organic Framework Functionalized Chiral Stationary Phase with Mixed-Mode Retention Mechanism. *J. Chromatogr. A* **2022**, *1662*, 462731. [CrossRef] [PubMed]
36. Fang, Z.L.; Zheng, S.R.; Tan, J.B.; Cai, S.L.; Fan, J.; Yan, X.; Zhang, W.G. Tubular Metal–Organic Framework-Based Capillary Gas Chromatography Column for Separation of Alkanes and Aromatic Positional Isomers. *J. Chromatogr. A* **2013**, *1285*, 132–138. [CrossRef] [PubMed]
37. Zheng, M.; Chen, J.; Zhang, L.; Cheng, Y.; Lu, C.; Liu, Y.; Singh, A.; Trivedi, M.; Kumar, A.; Liu, J. Metal Organic Frameworks as Efficient Adsorbents for Drugs from Wastewater. *Mater. Today Commun.* **2022**, *31*, 103514. [CrossRef]
38. Shi, C.; Zhao, Z.; Zhao, L.; Kushwaha, A.; Kumar, A.; Wang, J.; Pan, Y.; Muddassir, M.; Lan, Q. Porphyrin-Based Fe/La Metal-Organic Frameworks as Photocatalysts for Dye Photodegradation: Syntheses and Mechanism Investigation. *Inorg. Chem. Commun.* **2023**, *154*, 110920. [CrossRef]
39. Qin, N.; Pan, A.; Yuan, J.; Ke, F.; Wu, X.; Zhu, J.; Liu, J.; Zhu, J. One-Step Construction of a Hollow Au@Bimetal-Organic Framework Core-Shell Catalytic Nanoreactor for Selective Alcohol Oxidation Reaction. *ACS Appl. Mater. Interfaces* **2021**, *13*, 12463–12471. [CrossRef]
40. Jayaramulu, K.; Mukherjee, S.; Morales, D.M.; Dubal, D.P.; Nanjundan, A.K.; Schneemann, A.; Masa, J.; Kment, S.; Schuhmann, W.; Otyepka, M.; et al. Graphene-Based Metal-Organic Framework Hybrids for Applications in Catalysis, Environmental, and Energy Technologies. *Chem. Rev.* **2022**, *122*, 17241–17338. [CrossRef]
41. Zhou, Y.; Mao, Z.; Wang, W.; Yang, Z.; Liu, X. In-Situ Fabrication of Graphene Oxide Hybrid Ni-Based Metal-Organic Framework (Ni-MOFs@GO) with Ultrahigh Capacitance as Electrochemical Pseudocapacitor Materials. *ACS Appl. Mater. Interfaces* **2016**, *8*, 28904–28916. [CrossRef]
42. Liu, X.; Yang, H.; Diao, Y.; He, Q.; Lu, C.; Singh, A.; Kumar, A.; Liu, J.; Lan, Q. Recent Advances in the Electrochemical Applications of Ni-Based Metal Organic Frameworks (Ni-MOFs) and Their Derivatives. *Chemosphere* **2022**, *307*, 135729. [CrossRef]
43. Liu, T.; Tang, Q.; Lu, T.; Zhu, C.; Li, S.; Zhou, C.; Yang, H. Metal–Organic Frameworks-Based Membranes with Special Wettability for Oil–Water Separation: A Review. *Coatings* **2023**, *13*, 1241. [CrossRef]
44. Liang, L.; Chen, J.; Chen, X.; Wang, J.; Qiu, H. In Situ Synthesis of a GO/COFs Composite with Enhanced Adsorption Performance for Organic Pollutants in Water. *Environ. Sci. Nano* **2022**, *9*, 554–567. [CrossRef]
45. Yola, M.L.; Atar, N. Amperometric Galectin-3 Immunosensor-Based Gold Nanoparticle-Functionalized Graphitic Carbon Nitride Nanosheets and Core–Shell Ti-MOF@COFs Composites. *Nanoscale* **2020**, *12*, 19824–19832. [CrossRef] [PubMed]
46. Sesigur, F.; Sakar, D.; Yasa-Sahin, O.; Ocak, H.; Cankurtaran, O.; Bilgin-Eran, B.; Karaman, F. Thermodynamic and Surface Characterisation of (S)-5-Dodecycloxy-2-[[[4-(2-Methylbutoxy) Phenyl]Imino]Metheyl]Phenol Thermotropic Liquid Crystal by Inverse Gas Chromatography. *Liq. Cryst.* **2012**, *39*, 87–97. [CrossRef]
47. Cui, W.G.; Hu, T.L.; Bu, X.H. Metal–Organic Framework Materials for the Separation and Purification of Light Hydrocarbons. *Adv. Mater.* **2020**, *32*, 1806445. [CrossRef] [PubMed]

48. Wu, Y.; Chen, H.; Liu, D.; Xiao, J.; Qian, Y.; Xi, H. Effective Ligand Functionalization of Zirconium-Based Metal-Organic Frameworks for the Adsorption and Separation of Benzene and Toluene: A Multiscale Computational Study. *ACS Appl. Mater. Interfaces* **2015**, *7*, 5775–5787. [CrossRef]
49. González-Galán, C.; De Fez-Febré, M.; Giancola, S.; González-Cobos, J.; Vidal-Ferran, A.; Galán-Mascarós, J.R.; Balestra, S.R.G.; Calero, S. Separation of Volatile Organic Compounds in TAMOF-1. *ACS Appl. Mater. Interfaces* **2022**, *14*, 30772–30785. [CrossRef]
50. Yu, H.; Zang, J.; Guo, C.; Li, B.; Li, B.; Zhang, X.; Chen, T. Research Progress on Adsorption and Separation of Petroleum Hydrocarbon Molecules by Porous Materials. *Separations* **2023**, *10*, 17. [CrossRef]
51. Li, X.; Li, B.; Liu, M.; Zhou, Y.; Zhang, L.; Qiao, X. Core-Shell Metal-Organic Frameworks as the Mixed-Mode Stationary Phase for Hydrophilic Interaction/Reversed-Phase Chromatography. *ACS Appl. Mater. Interfaces* **2019**, *11*, 10320–10327. [CrossRef]
52. Zheng, H.; Zhang, J.; Ma, J.; Jia, Q. Engineering Magnetic Guanidyl-Functionalized Supramolecular Organic Framework for Efficient Enrichment of Global Phosphopeptides. *ACS Appl. Mater. Interfaces* **2020**, *12*, 57468–57476. [CrossRef]
53. Sinha Roy, K.; Goud, R.D.; Mazumder, A.; Chandra, B.; Purohit, A.K.; Palit, M.; Dubey, D.K. Triazine-Based Covalent Organic Framework: A Promising Sorbent for Efficient Elimination of the Hydrocarbon Backgrounds of Organic Sample for GC-MS and 1 H NMR Analysis of Chemical Weapons Convention Related Compounds. *ACS Appl. Mater. Interfaces* **2019**, *11*, 16027–16039. [CrossRef]
54. Jiang, Q.; Xu, P.; Feng, J.; Sun, M. Nanostructured Silver Coating as a Stationary Phase for Capillary Gas Chromatography. *Molecules* **2019**, *24*, 4491. [CrossRef]
55. Ban, S.; Van Laak, A.; De Jongh, P.E.; Van Der Eerden, J.P.J.M.; Vlugt, T.J.H. Adsorption Selectivity of Benzene/Propene Mixtures for Various Zeolites. *J. Phys. Chem. C* **2007**, *111*, 17241–17248. [CrossRef]
56. Pasban, A.; Mostafavi, S.M.; Malekzadeh, H.; Nazari, B.M. Quantitative Determination of LPG Hydrocarbons by Modified Packed Column Adsorbent of Gas Chromatography Via Full Factorial Design. *J. Nanoanal.* **2017**, *4*, 31–40. [CrossRef]
57. Speltini, A.; Merli, D.; Quartarone, E.; Profumo, A. Separation of Alkanes and Aromatic Compounds by Packed Column Gas Chromatography Using Functionalized Multi-Walled Carbon Nanotubes as Stationary Phases. *J. Chromatogr. A* **2010**, *1217*, 2918–2924. [CrossRef] [PubMed]
58. Schneider, W.; Bruderreck, H.; Halász, I. Gas Chromatographic Separation of Hydrocarbons (C1 to C8) by Carbon Number Using Packed Capillary Columns. *Anal. Chem.* **1964**, *36*, 1533–1540. [CrossRef]
59. Merli, D.; Speltini, A.; Ravelli, D.; Quartarone, E.; Costa, L.; Profumo, A. Multi-Walled Carbon Nanotubes as the Gas Chromatographic Stationary Phase: Role of Their Functionalization in the Analysis of Aliphatic Alcohols and Esters. *J. Chromatogr. A* **2010**, *1217*, 7275–7281. [CrossRef] [PubMed]
60. Habila, M.A.; Alothman, Z.A.; Ali, R.; Ghafar, A.A.; Hassouna, M.S.E.-D. Removal of Tartrazine Dye onto Mixed-Waste Activated Carbon: Kinetic and Thermodynamic Studies. *Clean* **2014**, *42*, 1824–1831. [CrossRef]
61. Ji, Z.; Majors, R.E.; Guthrie, E.J. Porous Layer Open-Tubular Capillary Columns: Preparations, Applications and Future Directions. *J. Chromatogr. A* **1999**, *842*, 115–142. [CrossRef]
62. Haddad, P.R.; Taraji, M.; Szücs, R. Prediction of Analyte Retention Time in Liquid Chromatography. *Anal. Chem.* **2021**, *93*, 228–256. [CrossRef]
63. Hinshaw, J.V. Practical Gas Chromatography. *LCGC N. Am.* **2013**, *31*, 932–937.
64. Fidan, İ.; Daşdan, D.Ş.; Karaman, F.; Kaban, Ş. Surface Characterization of Thiazolidinone Derivatives by Inverse Gas Chromatography. *Bulg. Chem. Commun.* **2017**, *49*, 742–749.
65. van de Kamer, J.H.; Gerritsma, K.W.; Wansink, E.J. Gas-Liquid Partition Chromatography: The Separation and Micro-Estimation of Volatile Fatty Acids from Formic Acid to Dodecanoic Acid. *Biochem. J.* **1955**, *61*, 174–176. [CrossRef]
66. Gutmann, F.; Simmons, L.M. A Theoretical Basis for the Antoine Vapor Pressure Equation. *J. Chem. Phys.* **1950**, *18*, 696–697. [CrossRef]
67. Yusuf, K.; Badjah-Hadj-Ahmed, A.Y.; Aqel, A.; Aouak, T.; ALOthman, Z.A. Zeolitic Imidazolate Framework-Methacrylate Composite Monolith Characterization by Inverse Gas Chromatography. *J. Chromatogr. A* **2016**, *1443*, 233–240. [CrossRef]
68. Papadopoulou, S.K.; Papaiconomou, N.; Baup, S.; Iojoiu, C.; Svecova, L.; Thivel, P.X. Surface Characterization of 1-Butyl-1-Ethylpiperidinium Bromide by Inverse Gas Chromatography. *J. Mol. Liq.* **2019**, *287*, 110945. [CrossRef]
69. Fowkes, F.M. Attractive Forces At Interfaces. *Ind. Eng. Chem.* **1964**, *56*, 40–52. [CrossRef]
70. Schultz, J.; Martin, C. The Role of the Interface in Carbon Fibre-Epoxy Compositest. *J. Adhes.* **1987**, *23*, 45–60. [CrossRef]
71. Dolatyari, L.; Yaftian, M.R.; Rostamnia, S. Removal of Uranium(VI) Ions from Aqueous Solutions Using Schiff Base Functionalized SBA-15 Mesoporous Silica Materials. *J. Environ. Manag.* **2016**, *169*, 8–17. [CrossRef] [PubMed]
72. Queiroz, M.F.; Melo, K.R.T.; Sabry, D.A.; Sassaki, G.L.; Rocha, H.A.O. Does the Use of Chitosan Contribute to Oxalate Kidney Stone Formation? *Mar. Drugs* **2014**, *13*, 141–158. [CrossRef] [PubMed]
73. Ali, R.; Aslam, Z.; Shawabkeh, R.A.; Asghar, A.; Hussein, I.A. BET, FTIR, and RAMAN Characterizations of Activated Carbon from Waste Oil Fly Ash. *Turk. J. Chem.* **2020**, *44*, 279. [CrossRef]
74. De Menezes, B.R.C.; Ferreira, F.V.; Silva, B.C.; Simonetti, E.A.N.; Bastos, T.M.; Cividanes, L.S.; Thim, G.P. Effects of Octadecylamine Functionalization of Carbon Nanotubes on Dispersion, Polarity, and Mechanical Properties of CNT/HDPE Nanocomposites. *J. Mater. Sci.* **2018**, *53*, 14311–14327. [CrossRef]
75. Ostrowska-Czubenko, J.; Pieróg, M.; Gierszewska-Drużyńska, M. State of water in noncrosslinked and crosslinked hydrogel chitosan membranes—Dsc studies. *Prog. Chem. Appl. Chitin Its Deriv.* **2011**, *16*, 147–156.

76. Bhatnagar, A.; Hogland, W.; Marques, M.; Sillanpää, M. An Overview of the Modification Methods of Activated Carbon for Its Water Treatment Applications. *Chem. Eng. J.* **2013**, *219*, 499–511. [CrossRef]
77. Farma, R.; Wahyuni, F.; Awitdrus. Physical Properties Analysis of Activated Carbon from Oil Palm Empty Fruit Bunch Fiber on Methylene Blue Adsorption. *J. Technomater. Phys.* **2019**, *1*, 69–75. [CrossRef]
78. Chester, T.L.; Coym, J.W. Effect of Phase Ratio on van't Hoff Analysis in Reversed-Phase Liquid Chromatography, and Phase-Ratio-Independent Estimation of Transfer Enthalpy. *J. Chromatogr. A* **2003**, *1003*, 101–111. [CrossRef] [PubMed]
79. Yang, Y.C.; Yoon, P.R. Determination of Acid-Base Properties of Silicas by Inverse Gas Chromatography: Variation with Surface Treatment. *Mater. Trans.* **2007**, *48*, 1955–1960. [CrossRef]
80. Denayer, J.F.; Baron, G.V.; Martens, J.A.; Jacobs, P.A. Chromatographic Study of Adsorption of N-Alkanes on Zeolites at High Temperatures. *J. Phys. Chem. B* **1998**, *102*, 3077–3081. [CrossRef]
81. Luebbers, M.T.; Wu, T.; Shen, L.; Masel, R.I. Trends in the Adsorption of Volatile Organic Compounds in a Large-Pore Metal-Organic Framework, IRMOF-1. *Langmuir* **2010**, *26*, 11319–11329. [CrossRef]
82. Gumrukcu, G.; Garikyan, S.; Keser Karaoglan, G.; Sakar, D. Structural and Surface Characterization of Newly Synthesized D-π-D Type Schiff Base Ligand: (1E,2E)-3-[4-(Dimethylamino)Phenyl]Prop-2-En-1-Ylidene) Phenylamine. *J. Chem.* **2013**, *2013*, 298205. [CrossRef]

Disclaimer/Publisher's Note: The statements, opinions and data contained in all publications are solely those of the individual author(s) and contributor(s) and not of MDPI and/or the editor(s). MDPI and/or the editor(s) disclaim responsibility for any injury to people or property resulting from any ideas, methods, instructions or products referred to in the content.